

Cite this: *Nanoscale Adv.*, 2021, 3, 4528

# Environmentally hazardous gas sensing ability of MoS<sub>2</sub>-nanotubes: an insight from the electronic structure and transport properties†

Nabajyoti Baidya,<sup>ID</sup>\*<sup>a</sup> Narendra Nath Ghosh<sup>ID</sup><sup>b</sup> and Asoke P. Chattopadhyay<sup>ID</sup><sup>a</sup>

Herein we have investigated the ability of the (6,6) MoS<sub>2</sub>-nanotube (NT) to sense environmentally hazardous electrophilic and nucleophilic gases using density functional theory (DFT). CO, CO<sub>2</sub>, H<sub>2</sub>O and NH<sub>3</sub> gases were chosen for adsorption on the (6,6) MoS<sub>2</sub>-NT and different adsorption parameters such as adsorption energy, projected density of states (PDOS), band structure and structural changes after adsorption were evaluated. Nucleophilic gases NH<sub>3</sub> and H<sub>2</sub>O showed a fairly high amount of electron density transfer from gas molecules to the NT while the opposite trend was realized for electrophilic gases CO and CO<sub>2</sub>. Among the four gases, H<sub>2</sub>O has the highest amount of adsorption energy (−1.74 eV) and a moderately high amount of charge transfer from H<sub>2</sub>O to the NT. Gas sensing behaviour was further rationalized from the enhanced *I*–*V* characteristics of gas adsorbed nanotubes compared to pristine ones. Analysis of results revealed that the (6,6) MoS<sub>2</sub>-NT showed a decent level of gas sensing properties towards CO, CO<sub>2</sub>, H<sub>2</sub>O and NH<sub>3</sub> gases, and high selectivity for H<sub>2</sub>O makes the MoS<sub>2</sub>-NT superior to previously reported MoS<sub>2</sub>-monolayer in this matter. These results suggest the possibility of fabrication of highly efficient MoS<sub>2</sub>-NT based gas sensors for environmentally hazardous gases.

Received 12th December 2020

Accepted 11th June 2021

DOI: 10.1039/d0na01037e

rsc.li/nanoscale-advances

## Introduction

Toxic and carcinogenic gases are the main contributors to air pollution. These gases can affect both human health and the environment directly or indirectly. Oxides of carbon, nitrogen and other elements, along with methane, ammonia, CFCs and water vapour in air are mainly responsible for air pollution leading to various pulmonary and other diseases. Global warming is another issue which we cannot ignore any more. In this context, gas sensors which are cost effective, easy to use and require low power to operate are very promising candidates. Lots of research endeavours to discover and design such efficacious gas sensing materials are being carried out.

Use of 2D-materials such as graphene, hexagonal boron nitride nanosheets and carbon NTs as gas sensing agents is decades old.<sup>1–4</sup> Graphene oxide can also be used as a gas sensor.<sup>5</sup> Graphene quantum dots have shown potential sensing ability for toxic gases.<sup>6</sup> In the last few years, 2D-materials of transition metal dichalcogenides (TMDs) *viz.* MX<sub>2</sub> (X = S, Se, Te) have drawn attention due to their potential gas sensing properties.<sup>7</sup> Among these TMDs, MoS<sub>2</sub> has gas sensing ability

comparable to graphene<sup>8,9</sup> and WS<sub>2</sub> can sense both toxic and non-toxic gases.<sup>10,11</sup>

Among the 2D-transition metal dichalcogenides (TMDs), MoS<sub>2</sub> has evoked keen interest to the researchers due to its use in various fields *e.g.* optics, microbiology, catalysis, electrical appliances, energy conversion, gas sensing and lubrication.<sup>7,12–17</sup> Both bulk and single-layer MoS<sub>2</sub> showed semiconducting nature with an indirect band gap of 1.23 eV and 1.8 eV, respectively.<sup>18,19</sup> In MoS<sub>2</sub>, the Mo-atom is sandwiched between two S-atoms through covalent bonds, while the monolayers are held together by weak van der Waals forces.<sup>20</sup> MoS<sub>2</sub> monolayer plays a key role in adsorbing and detecting gases such as NH<sub>3</sub>, NO, NO<sub>2</sub>, CO, H<sub>2</sub>O, CO<sub>2</sub>, CH<sub>4</sub>, *etc.* 7–9, which are hazardous to both the environment and human health. The adsorption behaviour of MoS<sub>2</sub> monolayer is also explained by measuring the electronic transport properties of gas adsorbed MoS<sub>2</sub> monolayer. The gas sensing ability of MoS<sub>2</sub>@gas monolayer is explained by changes in the rectification behaviour.<sup>11</sup> The adsorption of CO and H<sub>2</sub> gases on MoS<sub>2</sub> monolayer by creating sulphur vacancies, *i.e.* by defective MoS<sub>2</sub> monolayer, results in enhanced catalytic activity.<sup>20</sup> The adsorption power of MoS<sub>2</sub> monolayer was found to be enhanced by silver functionalization.<sup>21</sup> Transition metal (V, Nb, Ta, and Ni) doped MoS<sub>2</sub> monolayer additionally showed potential gas adsorption properties.<sup>22,23</sup> The effect of applied electric field on gas sensing by MoS<sub>2</sub> monolayer has also been reported.<sup>24</sup>

Semiconducting MoS<sub>2</sub>-NTs have a graphitic honeycomb structure. Single walled MoS<sub>2</sub>-NTs can be synthesized by

<sup>a</sup>Department of Chemistry, University of Kalyani, Kalyani 741235, India. E-mail: nabajyotibaidya@gmail.com; asoke@klyuniv.ac.in

<sup>b</sup>Department of Chemistry, University of Gour Banga, Mokdumpur, Malda, 732103, India. E-mail: ghosh.naren13@gmail.com

† Electronic supplementary information (ESI) available. See DOI: 10.1039/d0na01037e



heating ammonium thiomolybdate<sup>25</sup> or by applying the catalytic transport of C<sub>60</sub> with MoS<sub>2</sub> powder.<sup>26</sup> It has generally two forms: (i) armchair (*n,n*) and (ii) zigzag (*n,0*).<sup>24</sup> Among these two forms, the armchair (*n,n*) MoS<sub>2</sub>-NT shows an indirect band gap whereas the zigzag form shows a direct band gap. For the (*n,n*) MoS<sub>2</sub>-NT, the band gap increases with the increase in the magnitude of *n*.<sup>27</sup> MoS<sub>2</sub>-NT systems can sense NH<sub>3</sub> and NO<sub>2</sub> gases.<sup>28</sup> There are several reports on the variation of gas sensing properties of MoS<sub>2</sub>-monolayer along with some other TMD materials, but the atomistic description of gas sensing ability of MoS<sub>2</sub>-NTs is scarce.<sup>5,29,30</sup> In the present work, we have made a comprehensive analysis of the adsorption behaviour and gas sensing ability of the (6,6) MoS<sub>2</sub>-NT. Compared to other armchair (8,8; 10,10; 12,12; 14,14 with band gaps of 0.496, 0.783, 0.954, and 1.079 eV, respectively) and zig-zag (10,0; 12,0; 14,0 with band gaps of 0.225, 0.405, and 0.615 eV, respectively) MoS<sub>2</sub>-NTs, the (6,6) NT possesses a lower band gap (0.19 eV).<sup>27</sup> So modulation of the electronic properties by adsorption of different gases can be achieved more easily involving the (6,6) NT. Furthermore, the results of adsorption of CO, CO<sub>2</sub>, NH<sub>3</sub> and H<sub>2</sub>O on the (6,6) MoS<sub>2</sub>-NT are compared to those on 2D MoS<sub>2</sub>-monolayer (ML). Surprisingly, it was found that the MoS<sub>2</sub>-NT can act as a better gas sensing agent as compared to MoS<sub>2</sub>-monolayer. This is verified from the binding energy analysis and explained by changes in the physical and electronic structure and *I-V* characteristics of the gases after adsorption.

## Methodology

In the present work, the (6,6) MoS<sub>2</sub> armchair NT has been chosen for the adsorption of CO, CO<sub>2</sub>, NH<sub>3</sub> and H<sub>2</sub>O gases. A double- $\zeta$  plus (DZP) function basis set and a mesh cut-off of 300

Ry at 300 K electronic temperature were considered for geometry optimization. The Perdew–Burke–Ernzerhof (PBE)<sup>31</sup> type generalized gradient approximation (GGA) exchange–correlation functional is used in all calculations, as implemented in the SIESTA program suite.<sup>32,33</sup> Though the PBE functional underestimates the band gap, the results offered by the PBE functional are quite reasonable and cost effective as demonstrated by previous reports.<sup>34,35</sup> The density matrix convergence criterion is set at 10<sup>−4</sup>. The conjugate gradient method is used to stabilize all atoms until the maximum tolerance force reached a value less than 0.01 eV Å<sup>−1</sup>. A 1 × 1 × 6 Monkhorst–Pack *k*-grid with a vacuum more than 20 Å in the *x* and *y* directions is applied in order to decouple the adjacent mirror images. In the present study, a single gas molecule was considered for adsorption on the NT to avoid spurious interactions between two neighbouring adsorbate gases. The adsorption energies of the gases are calculated using the following equation:

$$E_{\text{ads.}} = E_{\text{nanotube+gas}} - E_{\text{nanotube}} - E_{\text{gas}} \quad (1)$$

where  $E_{\text{nanotube+gas}}$  indicates the total energy of the composite system and  $E_{\text{nanotube}}$  and  $E_{\text{gas}}$  are the energies of the MoS<sub>2</sub>-NT and the studied gases, respectively.

Furthermore, to understand the adsorption mechanism, electronic transport properties of the MoS<sub>2</sub>-NT and MoS<sub>2</sub>-NT@gases have been studied by applying density functional theory combined with non-equilibrium Green's function as implemented in TransSIESTA.<sup>34</sup> A similar correlation functional was used to calculate the transport properties as above. To study the transport properties of the MoS<sub>2</sub>-NT and MoS<sub>2</sub>-NT@gas, three regions were considered *viz.* the left hand electrode (LHE,

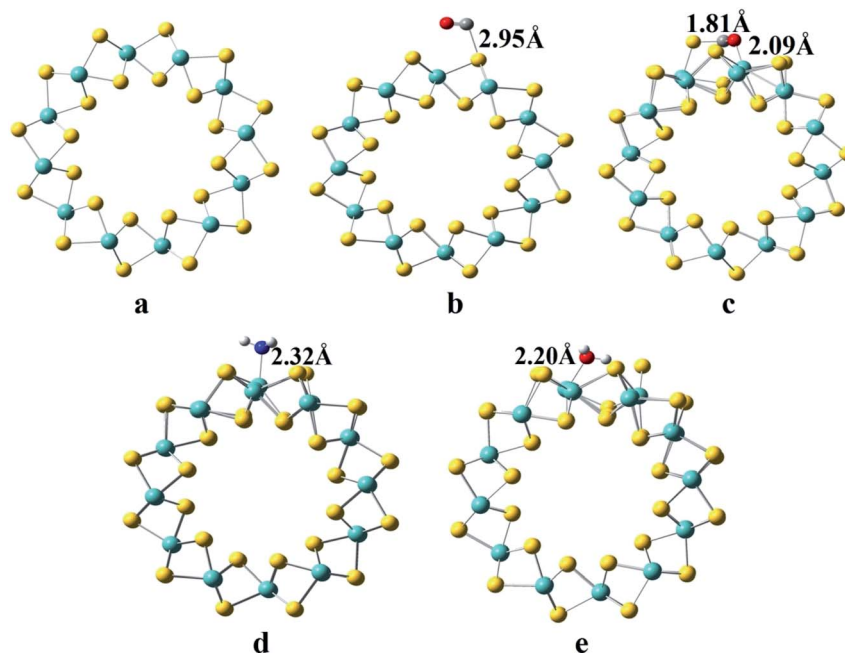


Fig. 1 Top view of the MoS<sub>2</sub>-NT and gas adsorbed MoS<sub>2</sub>-NT (a) MoS<sub>2</sub>-NT, (b) MoS<sub>2</sub>-NT@CO, (c) MoS<sub>2</sub>-NT@CO<sub>2</sub>, (d) MoS<sub>2</sub>-NT@NH<sub>3</sub>, and (e) MoS<sub>2</sub>-NT@H<sub>2</sub>O.



containing 36 atoms), right hand electrode (RHE, containing 36 atoms) and scattering region (SR, containing 140 atoms in the MoS<sub>2</sub>-NT, 142 atoms in MoS<sub>2</sub>-NT@CO, 143 atoms in MoS<sub>2</sub>-NT@CO<sub>2</sub>, 144 atoms in MoS<sub>2</sub>-NT@NH<sub>3</sub> and 143 atoms in MoS<sub>2</sub>-NT@H<sub>2</sub>O). Applying the Landauer–Buttiker formula under finite bias ( $V_b$ ), the amount of current passed was calculated within the energy bias window from  $-eV_b/2$  to  $+eV_b/2$  by integrating the transmission function  $T(E, V_b)$ .

$$I(V_b) = \frac{2e}{h} \int_{-\infty}^{+\infty} T(E, V_b) [f_L(E - \mu_L) - f_R(E - \mu_R)] dE \quad (2)$$

where  $f_L$  and  $f_R$  are the Fermi–Dirac distribution functions for the left and right electrodes, respectively and  $\mu_L$  and  $\mu_R$  are the chemical potentials of the left and right electrodes, respectively and  $eV_b = \mu_L - \mu_R$ . To understand the  $I$  vs.  $V$  characteristics, a finite bias from  $-1$  to  $1$  V was used keeping a bias spacing of  $0.1$  eV.

## Results and discussion

The optimized lattice parameter for the (6,6) MoS<sub>2</sub>-NT was found to be  $3.23 \text{ \AA}$ , which is much better than that found in previous theoretical studies.<sup>27</sup> Optimized structures of the (6,6) MoS<sub>2</sub>-NT itself and with CO, CO<sub>2</sub>, H<sub>2</sub>O and NH<sub>3</sub> adsorbed on it are shown in Fig. 1a–e. Four different adsorption sites *viz.* the top of the hexagon (the H-site), top of the outer S-atom (the S-site), top of the Mo-atom (the M-site) and top of a Mo–S bond site (the B-site) on the surface of the MoS<sub>2</sub>-NT were considered for gas adsorption. We note that for CO and CO<sub>2</sub> adsorption, the preferable sites are the H-site and S-site, respectively, while for NH<sub>3</sub> and H<sub>2</sub>O the preferable site is the M-site.

Fig. 2a shows the adsorption energies of the composite systems along with the favoured binding sites (values are available in Table S1†). The MoS<sub>2</sub>-NT@CO system has an adsorption energy of  $-0.44$  eV at the H-site; for the MoS<sub>2</sub>-

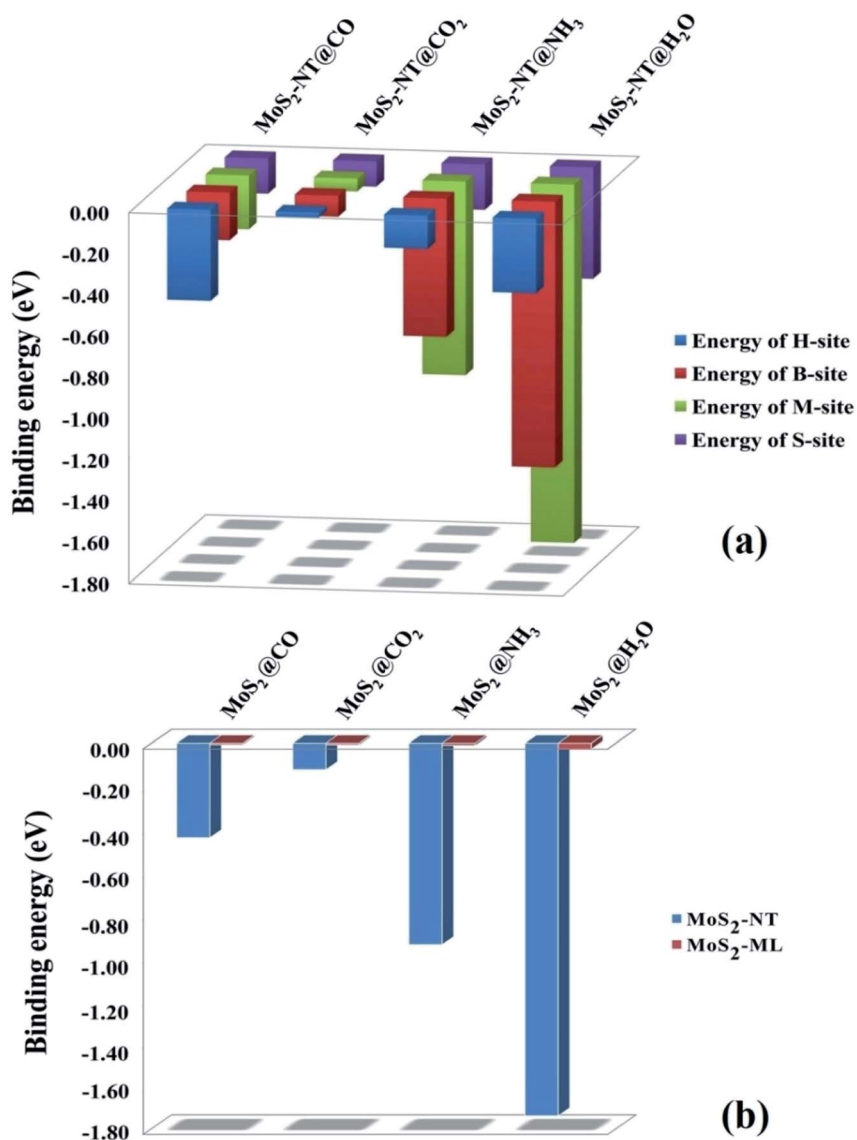


Fig. 2 (a) Adsorption energies of gases at different sites of the MoS<sub>2</sub>-NT, (b) adsorption energies of gases with the MoS<sub>2</sub>-NT and MoS<sub>2</sub>-ML.<sup>7</sup>



NT@CO<sub>2</sub> system, the adsorption energy at the S-site is  $-0.12$  eV and for MoS<sub>2</sub>-NT@NH<sub>3</sub> and MoS<sub>2</sub>-NT@H<sub>2</sub>O, where adsorption is on the M-site, the adsorption energy values are  $-0.94$  eV and  $-1.74$  eV, respectively.

The negative adsorption energies reveal that the adsorption is purely exothermic and therefore energetically favourable in all cases. Fig. 2b shows the comparison of adsorption energies between the MoS<sub>2</sub>-NT and MoS<sub>2</sub>-monolayer (ML)<sup>7</sup> which clearly indicates that the MoS<sub>2</sub>-NT shows greater adsorption energies compared to MoS<sub>2</sub>-ML (adsorption energies are given in Table S2, ESI†).

From the above figure, it is clear that the nucleophilic gases NH<sub>3</sub> and H<sub>2</sub>O are adsorbed more strongly on the (6,6) MoS<sub>2</sub>-NT yielding higher adsorption energies, while the electrophilic gases CO and CO<sub>2</sub> are less strongly adsorbed with lower adsorption energies. Analysis of bond lengths and adsorption energies revealed that the nucleophilic gases are adsorbed preferentially over the electrophilic sites on the (6,6) MoS<sub>2</sub>-NT, while electrophilic gases prefer to bind to the nucleophilic sites more. The bond distances of CO and CO<sub>2</sub> from their nearest sulphur atom of the MoS<sub>2</sub>-NT are 2.95 Å and 2.82 Å, respectively, while the bond distances of NH<sub>3</sub> and H<sub>2</sub>O from their nearest Mo atom are 2.32 Å and 2.20 Å, respectively. Higher values of adsorption energies of the nucleophilic gases are also understood from the Mulliken charge analysis. Fig. 3 enlists the Mulliken charges of the composite systems studied (data are listed in Table S3, ESI†).

It was found that, for NH<sub>3</sub> and H<sub>2</sub>O, 0.25 and 0.08 electronic charges were respectively transferred to the MoS<sub>2</sub>-NT on adsorption. However, 0.08 and 0.07 electronic charges were transferred from the MoS<sub>2</sub>-NT to the anti-bonding  $\pi^*$ -orbital of CO and CO<sub>2</sub> gases, respectively. The charge transfer from the MoS<sub>2</sub>-NT to CO and CO<sub>2</sub> is further understood from the elongation of the C–O bond from 1.14 Å to 1.15 Å in CO and from 1.17 Å to 1.28 Å in CO<sub>2</sub> as these gases are adsorbed on the MoS<sub>2</sub>-NT. Similarly, the charge transfer from MoS<sub>2</sub> to NH<sub>3</sub> and H<sub>2</sub>O is further evident from the elongation of the N–H bond from 1.02 Å to 1.03 Å in NH<sub>3</sub> and of the O–H bond from 0.97 Å to 1.02 Å in H<sub>2</sub>O along with the change in the bond angle in both NH<sub>3</sub> and H<sub>2</sub>O molecules, as these are adsorbed on the MoS<sub>2</sub>-NT.

The valence band maxima (VBM) and conduction band minima (CBM) of the composite systems are in accordance with the Mulliken charge analysis. Fig. 4 shows how the electrophilic

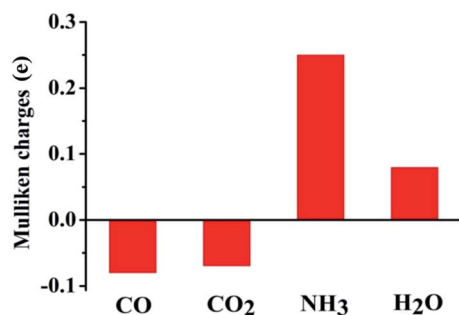


Fig. 3 Mulliken charges on gases adsorbed on the MoS<sub>2</sub>-NT.

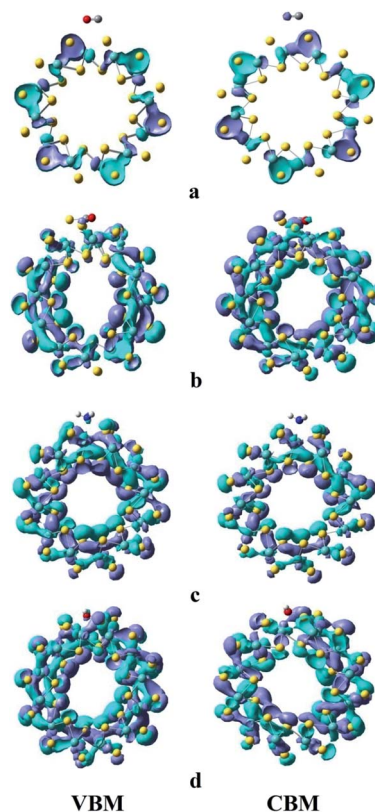


Fig. 4 Charge density isosurface (isovalue = 0.02) plot for MoS<sub>2</sub>-NT@gases: (a) MoS<sub>2</sub>-NT-CO, (b) MoS<sub>2</sub>-NT-CO<sub>2</sub>, (c) MoS<sub>2</sub>-NT-NH<sub>3</sub>, and (d) MoS<sub>2</sub>-NT-H<sub>2</sub>O.

and nucleophilic character of the gases affect the charge transfer from the MoS<sub>2</sub>-NT to gases and *vice versa*. The charge density distribution shown in Fig. 4 clearly demonstrates that a substantial amount of electron density is transferred from the NT to electrophilic CO and CO<sub>2</sub> while for NH<sub>3</sub> and H<sub>2</sub>O a reverse trend is observed.

Structural parameters of these gases before and after adsorption are presented in Table 1. The obtained results revealed a significant change in the structure of the gases after adsorption on the (6,6) MoS<sub>2</sub>-NT. Bond lengths of all gases are increased upon adsorption on the NT. Bond angles are also increased in CO<sub>2</sub>, NH<sub>3</sub> and H<sub>2</sub>O after adsorption. For CO and CO<sub>2</sub>, the bond lengths are increased by 0.01 Å and 0.11 Å, respectively, along with a change in the bond angle from 179.94° to 119.32° in the case of CO<sub>2</sub>. In the case of NH<sub>3</sub> and H<sub>2</sub>O, the bond lengths are increased by 0.01 Å and 0.05 Å, respectively, and the bond angles are increased by 2.40° and 0.75°, respectively, after adsorption.

The projected density of states (PDOS) of different gases adsorbed on the MoS<sub>2</sub>-NT is plotted in Fig. 5a–e to analyse the contribution arising from the gases and the MoS<sub>2</sub>-NT to the corresponding valence and conduction bands of the composite systems. It must be noted that the more electronegative S atom appears in the valence band while the more electropositive Mo atom contributes to the conduction band of the MoS<sub>2</sub>-NT. Furthermore, compared to the free MoS<sub>2</sub>-NT, the composite



Table 1 Structural changes of gases after adsorption on the MoS<sub>2</sub>-NT

Gas	Bond length in free gas (Å)	Bond angle in free gas (degree)	Bond length in adsorbed gas (Å)	Bond angle in adsorbed gas (degree)
CO	1.14	—	1.15	—
CO <sub>2</sub>	1.17	179.94	1.28	119.32
NH <sub>3</sub>	1.02	107.49	1.03	109.89
H <sub>2</sub> O	0.97	104.89	1.02	105.64

systems showed smaller band gaps. The nucleophilic NH<sub>3</sub> and H<sub>2</sub>O gases appear in the corresponding conduction band of the composite system due to the transfer of electron density from the gases to the conduction band of the MoS<sub>2</sub>-NT. With electrophilic gases, there is a significant charge transfer from the more electronegative sulphur of the MoS<sub>2</sub>-NT to the corresponding vacant orbital of the CO and CO<sub>2</sub> gases, resulting in the elongation of the C–O bond (bond length 1.14 to 1.15 Å) in CO while a change in hybridization from sp to sp<sup>2</sup> in CO<sub>2</sub>.

To analyze the performance of the MoS<sub>2</sub>-NT as a potential sensor, the non-equilibrium Green's function (NEGF) method is employed to evaluate the transport and corresponding current–voltage (*I*–*V*) characteristics of the MoS<sub>2</sub>-NT before and after gas adsorption. The model systems of the designed two semi-infinite electrodes along with the scattering region where the different gases were adsorbed are shown in Fig. 6.

A remarkable effect of gas adsorption on current–voltage characteristics is observed from the *I* vs. *V* curve as presented in

Fig. 7. For all gas adsorption cases, *I* vs. *V* showed a noticeable increase in current flow with respect to the pristine MoS<sub>2</sub>-NT. This increase in the current signal clearly indicates that there is a huge impact on the transport characteristics of the MoS<sub>2</sub>-NT after gas adsorption. Among the four different gas adsorption cases, the CO<sub>2</sub> adsorbed MoS<sub>2</sub>-NT showed enhanced current flow. However NH<sub>3</sub> and CO adsorbed MoS<sub>2</sub>-NTs showed almost a similar current flow, and the H<sub>2</sub>O adsorbed MoS<sub>2</sub>-NT showed the least current flow. A similar effect of NH<sub>3</sub> and CO adsorbed MoS<sub>2</sub>-NTs can be attributed to the similarity of the energy difference between the conduction and valence bands. On the other hand, the stronger effect of CO<sub>2</sub> adsorption on the transport characteristics can be explained from the large decrease of the CBM and VBM energy states. It is interesting to note that, though H<sub>2</sub>O is strongly adsorbed on the MoS<sub>2</sub>-NT (−1.74 eV) and there is a large decrease in the CBM and VBM levels, current flow is least affected by H<sub>2</sub>O adsorption. Such current–voltage behaviour for H<sub>2</sub>O and CO<sub>2</sub> adsorption can be

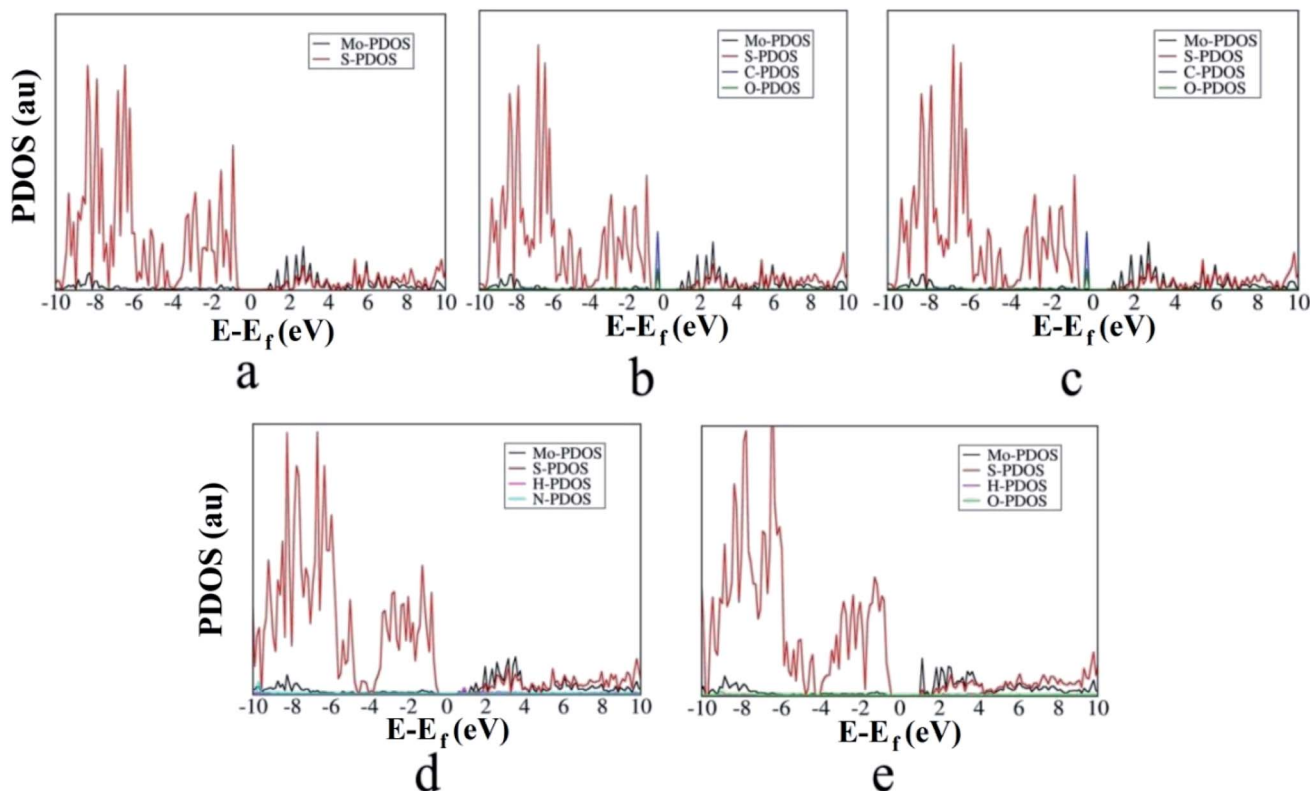


Fig. 5 PDOS of the (6,6) MoS<sub>2</sub>-NT and MoS<sub>2</sub>-NT@gases: (a) MoS<sub>2</sub>-NT, (b) MoS<sub>2</sub>-NT@CO, (c) MoS<sub>2</sub>-NT@CO<sub>2</sub>, (d) MoS<sub>2</sub>-NT@NH<sub>3</sub> and (e) MoS<sub>2</sub>-NT@H<sub>2</sub>O.



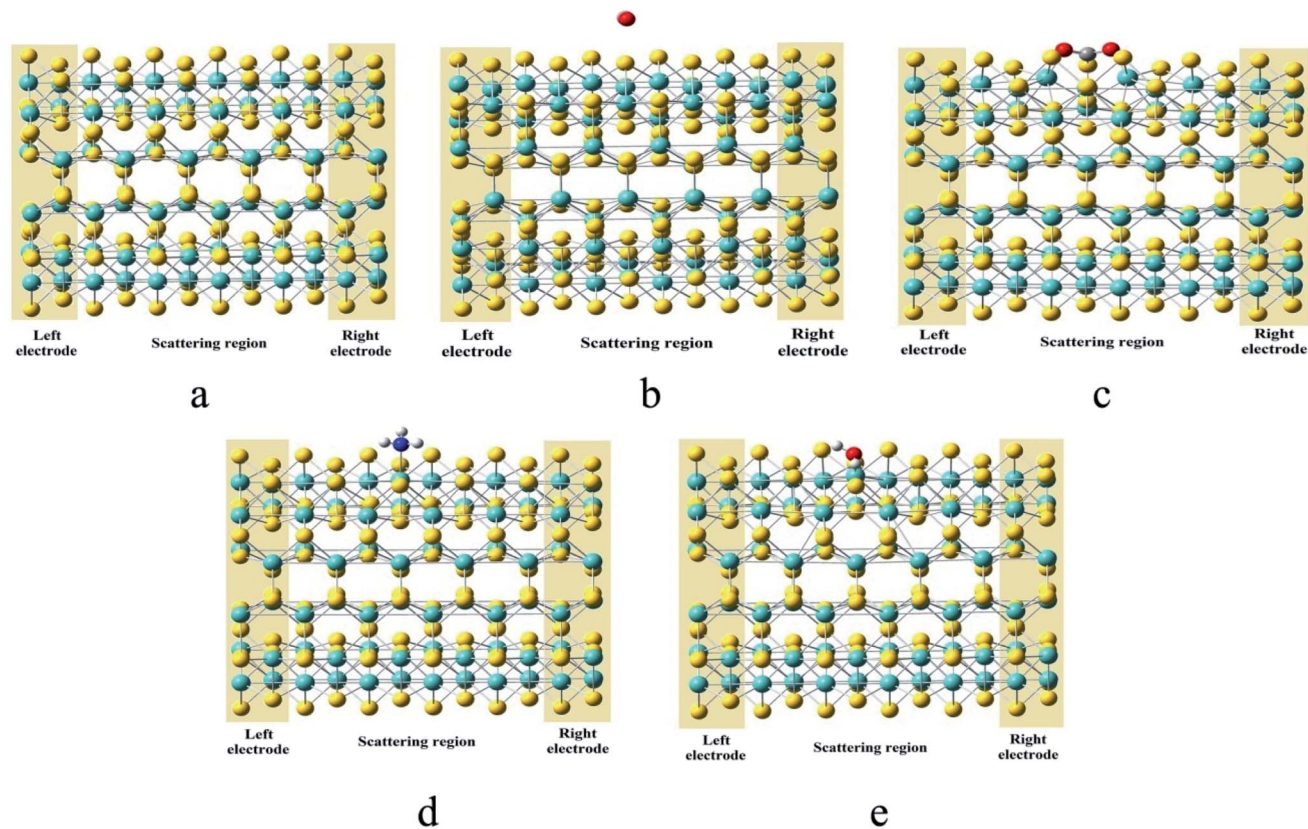


Fig. 6 Optimised geometries of (a) the MoS<sub>2</sub>-NT, (b) MoS<sub>2</sub>-NT@CO, (c) MoS<sub>2</sub>-NT@CO<sub>2</sub>, (d) MoS<sub>2</sub>-NT@NH<sub>3</sub>, and (e) MoS<sub>2</sub>-NT@H<sub>2</sub>O with electrodes and the scattering region.

interpreted by the inhibition of the conduction channel due to an appreciable amount of charge flow from H<sub>2</sub>O to the MoS<sub>2</sub>-NT.

The noticeable difference in the current signal due to gas adsorption can be regarded as a superior characteristic of the device modelling of MoS<sub>2</sub>-NT based gas sensors.

To better understand the shifting of conduction and valence bands due to charge transfer after adsorption of gases, we have

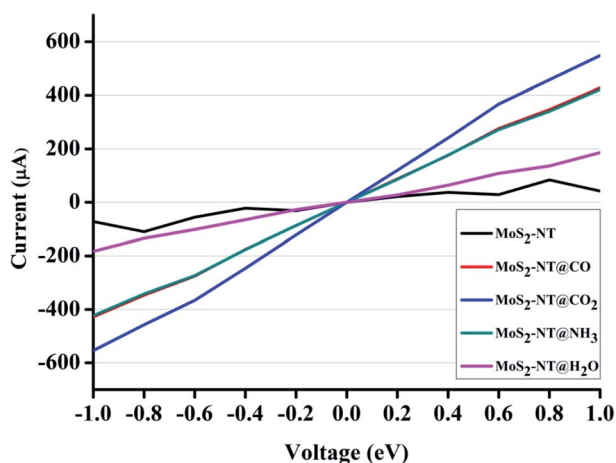


Fig. 7 *I* vs. *V* characteristics of the MoS<sub>2</sub>-NT, MoS<sub>2</sub>-NT@CO, MoS<sub>2</sub>-NT@CO<sub>2</sub>, MoS<sub>2</sub>-NT@NH<sub>3</sub> and MoS<sub>2</sub>-NT@H<sub>2</sub>O.

plotted the transmission function for bare and adsorbed NTs as shown in Fig. 8. Charge transfer in MoS<sub>2</sub>-NT@CO<sub>2</sub> from the MoS<sub>2</sub>-NT to CO<sub>2</sub> results in the shrinking of the transport bands and the transmission function shows a broad peak in conduction and valence bands. As a result, CO<sub>2</sub> adsorption increases the conduction channel in MoS<sub>2</sub>-NT@CO<sub>2</sub>, showing a broad current signal in the *I* vs. *V* window. On the other hand, charge transfer from H<sub>2</sub>O to the MoS<sub>2</sub>-NT shifts the conduction band to a lower energy, thereby inhibiting the conduction channel which shows lower transmission peaks. A similar behaviour in the current signal in the *I* vs. *V* window for MoS<sub>2</sub>-NT@NH<sub>3</sub> and MoS<sub>2</sub>-NT@CO has been attributed to the alignment of similar transport bands and transmission signals in valence and conduction bands.

Furthermore, to understand how adsorption affects the overall band structure of these systems, we have performed band structure analysis of the MoS<sub>2</sub>-NT and gas adsorbed MoS<sub>2</sub>-NT as shown in Fig. 9a–e. Fig. 9a revealed an indirect band gap of 0.19 eV for the free MoS<sub>2</sub>-NT. After gas adsorption, there is a profound impact on the band structure of the system.

After adsorption of different gases, the indirect band gap decreases in all cases. For MoS<sub>2</sub>-NT@CO, the band gap is 0.13 eV and for MoS<sub>2</sub>-NT@CO<sub>2</sub>, this band gap is reduced further to 0.04 eV. Again, in MoS<sub>2</sub>-NT@NH<sub>3</sub>, the band gap is 0.15 eV and for MoS<sub>2</sub>-NT@H<sub>2</sub>O, there is an overlap between the valence and conduction bands. For MoS<sub>2</sub>-NT@CO and MoS<sub>2</sub>-NT@CO<sub>2</sub>, the conduction bands become more dense compared to those of



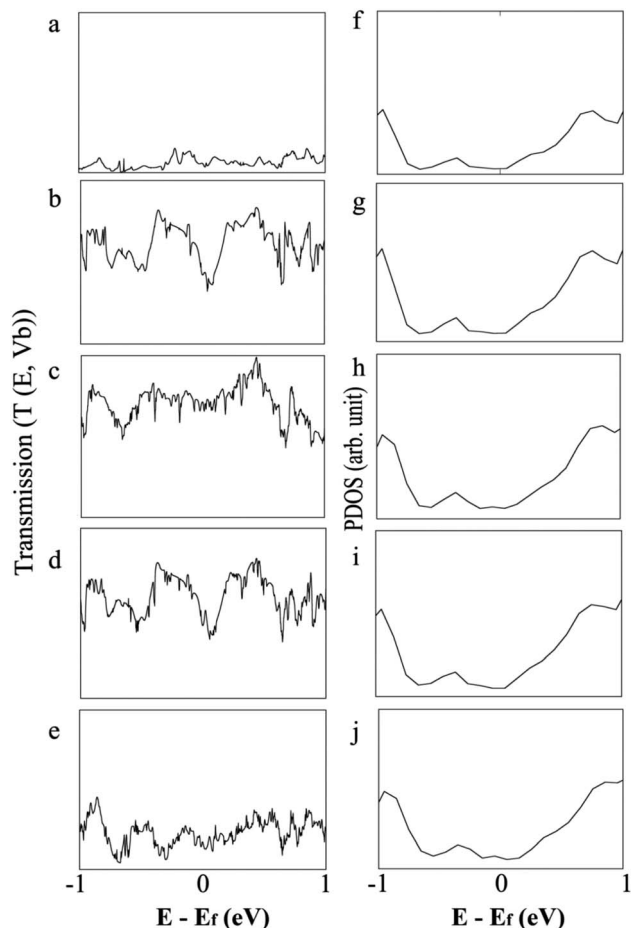


Fig. 8 Transmission function of (a) the MoS<sub>2</sub>-NT, (b) MoS<sub>2</sub>-NT@CO, (c) MoS<sub>2</sub>-NT@CO<sub>2</sub>, (d) MoS<sub>2</sub>-NT@NH<sub>3</sub>, (e) MoS<sub>2</sub>-NT@H<sub>2</sub>O and PDOS of (f) the MoS<sub>2</sub>-NT, (g) MoS<sub>2</sub>-NT@CO, (h) MoS<sub>2</sub>-NT@CO<sub>2</sub>, (i) MoS<sub>2</sub>-NT@NH<sub>3</sub>, (j) MoS<sub>2</sub>-NT@H<sub>2</sub>O.

MoS<sub>2</sub>-NT. Furthermore, in the case of MoS<sub>2</sub>-NT@NH<sub>3</sub> and MoS<sub>2</sub>-NT@H<sub>2</sub>O, the density of the conduction band is increased further. Hence the band structure is also in concordance with the Mulliken charge analysis and VBM-CBM analysis. Only in the case of MoS<sub>2</sub>-NT@H<sub>2</sub>O, the conduction band crosses the Fermi level, which is an indication of the metallic character of the system. It is also clear from the band structure that the MoS<sub>2</sub>-NT shows much stronger binding with H<sub>2</sub>O. Thus the

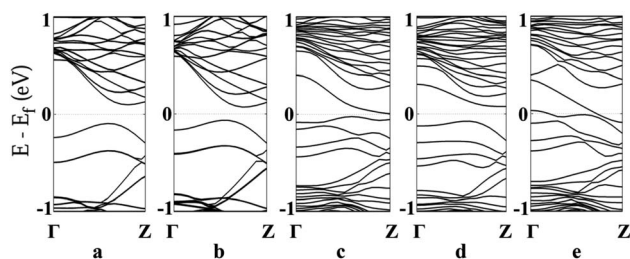


Fig. 9 Band structure of the MoS<sub>2</sub>-NT and MoS<sub>2</sub>-NT@gases: (a) MoS<sub>2</sub>-NT, (b) MoS<sub>2</sub>-NT@CO, (c) MoS<sub>2</sub>-NT@CO<sub>2</sub>, (d) MoS<sub>2</sub>-NT@NH<sub>3</sub> and (e) MoS<sub>2</sub>-NT@H<sub>2</sub>O.

band structures also explain the binding nature of the gases on the MoS<sub>2</sub>-NT.

## Conclusions

In the present work, the adsorption of environmentally hazardous gases on the (6,6)-MoS<sub>2</sub>-NT was analysed from their electronic structure and transport properties. Binding is controlled by the electrophilic and nucleophilic characters of the gases, which also govern charge transfer to and from the MoS<sub>2</sub>-NT. The electrophilic character of CO and CO<sub>2</sub> lead to charge transfer from the NT to these gases, whereas the nucleophilic character of NH<sub>3</sub> and H<sub>2</sub>O showed the reverse trend. These gases, upon adsorption on the MoS<sub>2</sub>-NT, are activated, as evident from the structural changes in these gases. These phenomena are explained by Mulliken charge analysis, VBM-CBM analysis, *I* vs. *V* characteristics, transmission function, PDOS and band structure analysis. The presence of more electronegative atoms on the molecule also controls the binding energy and the band structure of the systems studied. Analysis of data reveals that compared to MoS<sub>2</sub>-ML, the MoS<sub>2</sub>-NT showed enhanced gas sensing ability and distinct *I*-*V* characteristics, which suggests the fabrication of new gas sensing devices from the MoS<sub>2</sub> based NT.

## Data availability

Data are available upon request to the corresponding author.

## Author contributions

Nabajyoti Baildya: conceptualization, planning, writing. Narendranath Ghosh: conceptualization, execution, writing. Asoke P. Chattopadhyay: planning, supervision, writing.

## Conflicts of interest

The authors declare no conflicting interest among themselves regarding the present work.

## Acknowledgements

The authors wish to acknowledge infrastructural support from the Department of Chemistry, University of Kalyani, Kalyani, Nadia, India.

## References

- 1 K. S. Novoselov, D. Jiang, F. Schedin, T. Booth, V. Khotkevich, S. Morozov and A. K. Geim, Two-dimensional atomic crystals, *Proc. Natl. Acad. Sci. U. S. A.*, 2005, **102**(30), 10451–10453.
- 2 C. Lee, Q. Li, W. Kalb, X.-Z. Liu, H. Berger, R. W. Carpick and J. Hone, Frictional characteristics of atomically thin sheets, *science*, 2010, **328**(5974), 76–80.
- 3 L. Ci, L. Song, C. Jin, D. Jariwala, D. Wu, Y. Li, A. Srivastava, Z. Wang, K. Storr and L. Balicas, Atomic layers of hybridized



- boron nitride and graphene domains, *Nat. Mater.*, 2010, **9**(5), 430–435.
- 4 Y. Wang and J. T. Yeow, A review of carbon nanotubes-based gas sensors, *J. Sens.*, 2009, 2009.
  - 5 M. Donarelli and L. Ottaviano, 2D materials for gas sensing applications: A review on graphene oxide, MoS<sub>2</sub>, WS<sub>2</sub> and phosphorene, *Sensors*, 2018, **18**(11), 3638.
  - 6 D. Raeyani, S. Shojaei and S. AhmadiKandjani, Optical graphene quantum dots gas sensors: experimental study, *Mater. Res. Express*, 2020, **7**(1), 015608.
  - 7 S. Zhao, J. Xue and W. Kang, Gas adsorption on MoS<sub>2</sub> monolayer from first-principles calculations, *Chem. Phys. Lett.*, 2014, **595**, 35–42.
  - 8 B. Cho, J. Yoon, S. K. Lim, A. R. Kim, D.-H. Kim, S.-G. Park, J.-D. Kwon, Y.-J. Lee, K.-H. Lee and B. H. Lee, Chemical sensing of 2D graphene/MoS<sub>2</sub> heterostructure device, *ACS Appl. Mater. Interfaces*, 2015, **7**(30), 16775–16780.
  - 9 J. Ren, H. Liu, Y. Xue and L. Wang, Adsorption Behavior of CH<sub>4</sub> Gas Molecule on the MoX<sub>2</sub> (S, Se, Te) Monolayer: The DFT Study, *Nanoscale Res. Lett.*, 2019, **14**(1), 293.
  - 10 V. Babar, H. Vovusha and U. Schwingenschlögl, Density Functional Theory Analysis of Gas Adsorption on Monolayer and Few Layer Transition Metal Dichalcogenides: Implications for Sensing, *ACS Appl. Nano Mater.*, 2019, **2**(9), 6076–6080.
  - 11 J. Sun, N. Lin, H. Ren, C. Tang, L. Yang and X. Zhao, Gas adsorption on MoS<sub>2</sub>/WS<sub>2</sub> in-plane heterojunctions and the I–V response: a first principles study, *RSC Adv.*, 2016, **6**(21), 17494–17503.
  - 12 E. Gourmelon, O. Lignier, H. Hadouda, G. Couturier, J. Bernède, J. Tedd, J. Pouzet and J. Salardenne, MS<sub>2</sub> (M= W, Mo) photosensitive thin films for solar cells, *Sol. Energy Mater. Sol. Cells*, 1997, **46**(2), 115–121.
  - 13 V. Yadav, S. Roy, P. Singh, Z. Khan and A. Jaiswal, 2D MoS<sub>2</sub>-based nanomaterials for therapeutic, bioimaging, and biosensing applications, *Small*, 2019, **15**(1), 1803706.
  - 14 T. F. Jaramillo, K. P. Jørgensen, J. Bonde, J. H. Nielsen, S. Horch and I. Chorkendorff, Identification of active edge sites for electrochemical H<sub>2</sub> evolution from MoS<sub>2</sub> nanocatalysts, *science*, 2007, **317**(5834), 100–102.
  - 15 Y. Li, H. Wang, L. Xie, Y. Liang, G. Hong and H. Dai, MoS<sub>2</sub> nanoparticles grown on graphene: an advanced catalyst for the hydrogen evolution reaction, *J. Am. Chem. Soc.*, 2011, **133**(19), 7296–7299.
  - 16 B. Radisavljevic, A. Radenovic, J. Brivio, V. Giacometti and A. Kis, Single-layer MoS<sub>2</sub> transistors, *Nat. Nanotechnol.*, 2011, **6**(3), 147–150.
  - 17 W. Wu, L. Wang, Y. Li, F. Zhang, L. Lin, S. Niu, D. Chenet, X. Zhang, Y. Hao and T. F. Heinz, Piezoelectricity of single-atomic-layer MoS<sub>2</sub> for energy conversion and piezotronics, *Nature*, 2014, **514**(7523), 470–474.
  - 18 K. Kam and B. Parkinson, Detailed photocurrent spectroscopy of the semiconducting group VIB transition metal dichalcogenides, *J. Phys. Chem.*, 1982, **86**(4), 463–467.
  - 19 K. F. Mak, C. Lee, J. Hone, J. Shan and T. F. Heinz, Atomically thin MoS<sub>2</sub>: a new direct-gap semiconductor, *Phys. Rev. Lett.*, 2010, **105**(13), 136805.
  - 20 D. Le, T. B. Rawal and T. S. Rahman, Single-layer MoS<sub>2</sub> with sulfur vacancies: structure and catalytic application, *J. Phys. Chem. C*, 2014, **118**(10), 5346–5351.
  - 21 J. Song and H. Lou, Improvement of gas-adsorption performances of Ag-functionalized monolayer MoS<sub>2</sub> surfaces: A first-principles study, *J. Appl. Phys.*, 2018, **123**(17), 175303.
  - 22 H. Wei, Y. Gui, J. Kang, W. Wang and C. Tang, A DFT study on the adsorption of H<sub>2</sub>S and SO<sub>2</sub> on Ni doped MoS<sub>2</sub> monolayer, *Nanomaterials*, 2018, **8**(9), 646.
  - 23 Q. Yue, Z. Shao, S. Chang and J. Li, Adsorption of gas molecules on monolayer MoS<sub>2</sub> and effect of applied electric field, *Nanoscale Res. Lett.*, 2013, **8**(1), 425.
  - 24 G. Seifert, H. Terrones, M. Terrones, G. Jungnickel and T. Frauenheim, Structure and electronic properties of MoS<sub>2</sub> nanotubes, *Phys. Rev. Lett.*, 2000, **85**(1), 146.
  - 25 M. Nath, A. Govindaraj and C. N. R. Rao, Simple synthesis of MoS<sub>2</sub> and WS<sub>2</sub> nanotubes, *Adv. Mater.*, 2001, **13**(4), 283–286.
  - 26 M. Remskar, A. Mrzel, Z. Skraba, A. Jesih, M. Ceh, J. Demšar, P. Stadelmann, F. Lévy and D. Mihailovic, Self-assembly of subnanometer-diameter single-wall MoS<sub>2</sub> nanotubes, *Science*, 2001, **292**(5516), 479–481.
  - 27 R. Ansari, S. Malakpour, M. Faghinihasiri and S. Sahmani, An *ab initio* investigation into the elastic, structural and electronic properties of MoS<sub>2</sub> nanotubes, *Superlattices Microstruct.*, 2015, **82**, 188–200.
  - 28 G. Deokar, P. Vancso, R. Arenal, F. Ravoux, J. Casanova-Cháfer, E. Llobet, A. Makarova, D. Vyalikh, C. Struzzi and P. Lambin, MoS<sub>2</sub>-carbon nanotube hybrid material growth and gas sensing, *Adv. Mater. Interfaces*, 2017, **4**(24), 1700801.
  - 29 Y. Niu, R. Wang, W. Jiao, G. Ding, L. Hao, F. Yang and X. He, MoS<sub>2</sub> graphene fiber based gas sensing devices, *Carbon*, 2015, **95**, 34–41.
  - 30 S. Cui, Z. Wen, X. Huang, J. Chang and J. Chen, Stabilizing MoS<sub>2</sub> nanosheets through SnO<sub>2</sub> nanocrystal decoration for high-performance gas sensing in air, *Small*, 2015, **11**(19), 2305–2313.
  - 31 J. P. Perdew, K. Burke and M. Ernzerhof, Generalized gradient approximation made simple, *Phys. Rev. Lett.*, 1996, **77**(18), 3865.
  - 32 E. Artacho, E. Anglada, O. Diéguez, J. D. Gale, A. García, J. Junquera, R. M. Martin, P. Ordejón, J. M. Pruneda and D. Sánchez-Portal, The SIESTA method; developments and applicability, *J. Phys.: Condens. Matter*, 2008, **20**(6), 064208.
  - 33 J. M. Soler, E. Artacho, J. D. Gale, A. García, J. Junquera, P. Ordejón and D. Sánchez-Portal, The SIESTA method for *ab initio* order-N materials simulation, *J. Phys.: Condens. Matter*, 2002, **14**(11), 2745.
  - 34 G. Sivaraman, F. b. A. de Souza, R. G. Amorim, W. L. Scopel, M. Fyta and R. H. Scheicher, Electronic transport along hybrid MoS<sub>2</sub> monolayers, *J. Phys. Chem. C*, 2016, **120**(41), 23389–23396.
  - 35 P. Bonardi, S. Achilli, G. F. Tantardini and R. Martinazzo, Electron transport in carbon wires in contact with Ag electrodes: a detailed first principles investigation, *Phys. Chem. Chem. Phys.*, 2015, **17**(28), 18413–18425.

